Inorganic Chemistry

Article

pubs.acs.org/IC

Multiply Bonded Metal(II) Acetate (Rhodium, Ruthenium, and Molybdenum) Complexes with the *trans*-1,2-Bis(*N*-methylimidazol-2-yl)ethylene Ligand

Nico Fritsch,[†,‡] Christian R. Wick,[‡,§] Thomas Waidmann,[†] Pavlo O. Dral,[§,⊥] Johannes Tucher,[†,∥] Frank W. Heinemann,[†] Tatyana E. Shubina,[§] Timothy Clark,*[,§] and Nicolai Burzlaff*[,†]

[†]Inorganic Chemistry and Interdisciplinary Center for Molecular Materials, Department of Chemistry and Pharmacy, Friedrich-Alexander-Universität Erlangen−Nürnberg, Egerlandstraße 1, 91058 Erlangen, Germany

[§]Computer-Chemie-Centrum and Interdisciplinary Center for Molecular Materials, Department of Chemistry and Pharmacy, Friedrich-Alexander-Universität Erlangen−Nürnberg, Nägelsbachstraße 25, 91052 Erlangen, Germany

Supporting Information

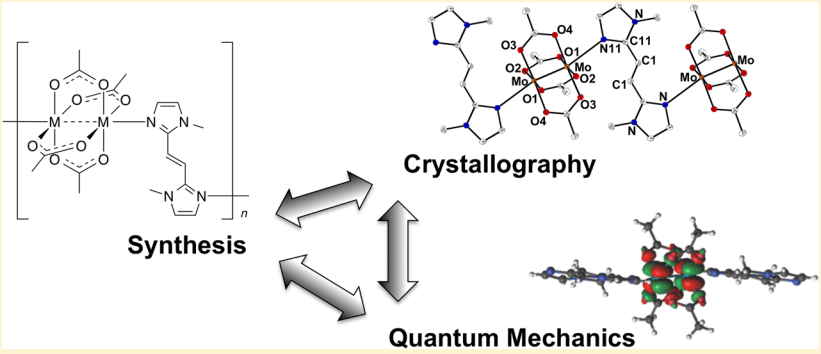

ABSTRACT: The synthesis and structural characterization of new coordination polymers with the *N*,*N*-donor ligand *trans*-1,2-bis(*N*-methylimidazol-2-yl)ethylene (*trans*-bie) are reported. It was found that the acetate-bridged paddlewheel metal(II) complexes $[M_2(O_2CCH_3)_4(trans\text{-bie})]_n$ with M = Rh, Ru, Mo, and Cr are linked by the *trans*-bie ligand to give a one-dimensional alternating chain. The metal−metal multiple bonds were analyzed with density functional theory and CASSCF/CASPT2 calculations (bond orders: Rh, 0.8; Ru, 1.7; Mo, 3.3).

INTRODUCTION

The use of transition-metal complexes to construct predictable, multidimensional networks has received ever-increasing attention in recent years.[1] The simplest topological coordination structure is a one-dimensional (1D) coordination polymer.[2] They, on the one hand, are easily accessible by self-assembly processes and, on the other hand, offer a wide range of functional properties.[3] One type of 1D coordination polymers is based on dinuclear metal units, which can be linked in various ways. An overview not only of polymers but also of dinuclear metal complexes in general is given by Cotton and co-workers.[4] One of the structural motives that have emerged is the paddlewheel structure. Generally this consists of two metal centers connected by four ligands, e.g., acetate groups. These dinuclear units can be linked together to obtain a 1D coordination polymer. The paddlewheel structure in its general features demands proximity of the metal atoms but does not of itself ensure or require a bonding interaction between them. This property makes this type of structure particularly interesting. It establishes a framework within the metal−metal interaction that can occur readily, but the nature and extent of the interaction can vary within the widest limits, depending upon the properties of the metal atoms concerned.[5]

We previously reported the synthesis of the new *N*,*N*-donor ligand *trans*-1,2-bis(*N*-methylimidazol-2-yl)ethylene (*trans*-bie) and its corresponding copper(II) acetate complex $[Cu_2(O_2CCH_3)_4(trans\text{-bie})]_n$.[6]

We now report the synthesis of new paddlewheel complexes of different metal(II) acetates (M = Rh, Ru, Mo, Cr) inspired by this copper(II)-based coordination polymer (Scheme 1). Our intention is to use the different M−M bonding characteristics found in the acetates to enable the rational synthesis of 1D coordination polymers with different types of M−M bonds. For example, the M−M (Cu−Cu) distance of 2.69 Å in $[Cu_2(O_2CCH_3)_4(trans\text{-bie})]_n$ did not indicate a significant bonding interaction between the copper centers, which is consistent with what is known about similar compounds.[6,7] Furthermore, for instance, Buslaev et al. found a Rh−Rh distance of 2.38 Å in rhodium(II) acetate, which indicates significant Rh−Rh bonding.[8] Similarly, Dunbar et al.[9]

Received: June 17, 2014
Published: November 13, 2014

   dx.doi.org/10.1021/ic501435a | *Inorg. Chem.* 2014, 53, 12305−12314

Scheme 1. Synthesis of 1D Coordination Polymer by the Self-assembly of *trans*-bie with Metal(II) Acetate[6]

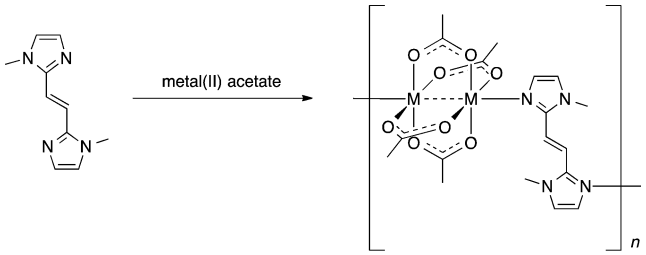

reported M−M double bonds in ruthenium(II) carboxylate compounds. The series is completed by the quadruply bonded chromium(II) and molybdenum(II) acetates.[10] The bonding between the transition metals is influenced strongly by the framework of the complex. Unfortunately, a bond order is neither physically observable nor uniquely defined. Among the different attempts that have been made to extract bond orders from theoretical calculations, those based on multiconfigurational molecular orbital theory and density functional theory (DFT) are commonly used for transition-metal dimers.[11] Such bond orders can differ significantly from standard integer bond orders.[11f,12] In multiconfigurational complete-active-space self-consistent-field (CASSCF) calculations, bond orders can be quantified by the effective bond order (EBO) introduced by Roos and co-workers.[11b,12] The EBO is the difference between the occupation numbers of the orbitals in a corresponding bonding and antibonding molecular orbital pair. The occupation numbers of natural orbitals obtained from a CASSCF wave function are not necessarily integers but rather noninteger values between 0 and 2. Therefore, the EBO obtained can be a noninteger value equal to or lower than the bond order expected from restricted molecular orbital or DFT theory. The Mayer bond order (MBO),[13] which can be used to quantify the bonding within DFT, has emerged as a useful tool, especially in inorganic chemistry.[14] In order to be able to compare results with earlier studies, we will focus on these two methods in our analyses of the complexes described.

We will first discuss the synthesis of the new dinuclear paddlewheel complexes with *trans*-bie and their experimental characterization. We will then analyze the crystal structures further by multiconfigurational molecular orbital theory and DFT to elucidate the influence of the ligands on the M−M bonds.

RESULTS AND DISCUSSION

Polymers. The polymeric complexes **1**−**3** were prepared by the addition of the *trans*-bie[6] ligand to the corresponding metal(II) acetate. Elemental analyses showed that all of the resulting complexes exhibit the stoichiometry of 1:1 $[M_2(O_2CCH_3)_4]$/*trans*-bie. The IR spectra of powder samples (KBr pellets) of all compounds exhibit the O−C−O vibrations as a set of two distinctive bands in a region very similar to that of the corresponding starting materials (Table 1). The Δ values of the asymmetric and symmetric O−C−O vibrations indicate the presence of bridging acetate groups.[15] The Δ values of the starting materials and the corresponding polymers are almost the same. Furthermore, they are all in the range proposed for bridged compounds[15] and also for molybdenum, which is known to have smaller values,[10a] and are in agreement with the Δ values calculated with DFT.

Table 1. Summary of Observed Vibrational Bands (KBr) of the Polymeric Complexes 1−3

polymer	$\tilde{\nu}_{asym}$(OCO) [cm^{-1}]	$\tilde{\nu}_{sym}$(OCO) [cm^{-1}]	Δ_{exp} [cm^{-1}]	Δ_{theo}[a] [cm^{-1}]
$[Rh_2(O_2CCH_3)_4$(*trans*-bie)$]_n$ (**1**)	1592	1420	172	192
$[Ru_2(O_2CCH_3)_4$(*trans*-bie)$]_n$ (**2**)	1569	1429	140	140
$Mo_2(O_2CCH_3)_4$(*trans*-bie)$]_n$ (**3**)	1527	1433	94	96

[a]B3LYP/def2-TZVP, scaled by 0.959 (see the SI).

This suggests that the dimer skeletons are preserved upon reaction with the bidentate ligand *trans*-bie to form linear coordination polymers comparable to $[Cu_2(O_2CCH_3)_4$(*trans*-bie)$]_n$.[6,10a] Crystals suitable for X-ray structure determination of complex $[Rh_2(O_2CCH_3)_4$(*trans*-bie)$]_n$ (**1**) were obtained by layering rhodium(II) acetate in tetrahydrofuran (THF) with *trans*-bie in methanol (MeOH). Crystals suitable for X-ray structure determination of $[Ru_2(O_2CCH_3)_4$(*trans*-bie)$]_n$ (**2**) and $[Mo_2(O_2CCH_3)_4$(*trans*-bie)$]_n$ (**3**) were obtained by layering the metal(II) acetate in THF with *trans*-bie in acetonitrile (MeCN). The molecular structures are shown in Figures1−3.

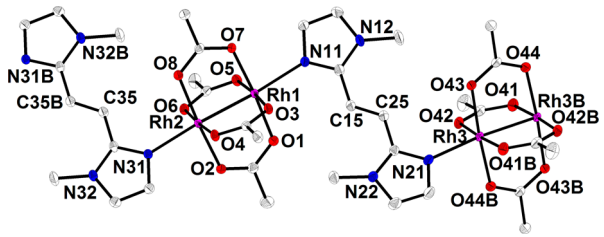

Figure 1. Cutout of the molecular structure of **1**. Thermal ellipsoids are drawn at the 50% probability level, and hydrogen atoms and MeOH molecules have been omitted for clarity.

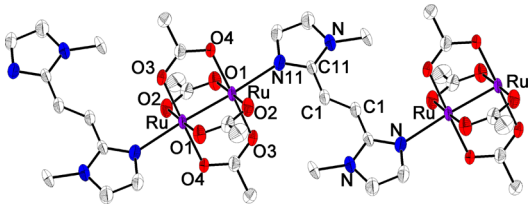

Figure 2. Cutout of the molecular structure of **2**. Thermal ellipsoids are drawn at the 50% probability level, and hydrogen atoms and THF molecules have been omitted for clarity.

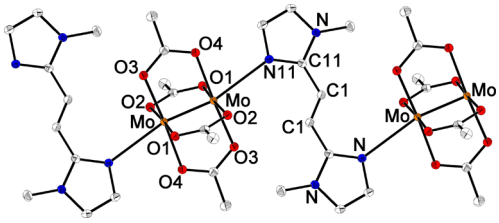

Figure 3. Cutout of the molecular structure of **3**. Thermal ellipsoids are drawn at the 50% probability level, and hydrogen atoms have been omitted for clarity.

dx.doi.org/10.1021/ic501435a | *Inorg. Chem.* 2014, 53, 12305−12314

An infinite chain of $[M_2(O_2CCH_3)_4]$ units bridged by the *N*,*N*-donor ligand *trans*-bie is found in all three structures. The paddlewheel unit consists of two metal centers μ-bridged by four acetato ligands. Each metal atom in this unit has a distorted square-pyramidal environment with four acetate oxygen atoms that form the equatorial base plane and one nitrogen atom of the *trans*-bie ligand. An inversion center is found in the middle of the double bond that connects the two imidazole groups in every second ligand in compound **1**. Further inversion centers exist in every second paddlewheel unit at the center of the Rh−Rh bond. Compounds **2** and **3** both exhibit two inversion centers in every ligand and paddlewheel unit. The M−M bond distances suggest single Rh−Rh, double Ru−Ru, and quadruple Mo−Mo bonds, as expected from the starting acetate complexes.[16] The M−O bond lengths are very similar in all polymer complexes. The M−M−N bond angle deviates more strongly from linearity from Rh to Ru and to Mo. The M−M and M−N distances of all chain complexes are summarized in Table 2.

Table 2. Structural Parameters of $[M_2(O_2CCH_3)_4$(*trans*-bie)$]_n$ (1−3) and $[Cu_2(O_2CCH_3)_4$(*trans*-bie)$]_n$

complex	M−M [Å]	M−N [Å]	M−M−N [deg]
$[Cu_2(O_2CCH_3)_4$(*trans*-bie)$]_n$[6]	2.6868(4)	2.1540(16)	172.07(5)
$[Rh_2(O_2CCH_3)_4$(*trans*-bie)$]_n$ (**1**)	2.4105(4), 2.4119(5)	2.224(2), 2.256(2), 2.253(3)	176.34(6), 174.27(7), 175.89(7)
$[Ru_2(O_2CCH_3)_4$(*trans*-bie)$]_n$ (**2**)	2.2829(11)	2.325(7)	173.89(17)
$[Mo_2(O_2CCH_3)_4$(*trans*-bie)$]_n$ (**3**)	2.1099(2)	2.7032(11)	163.32(2)

For further investigation, the solid UV/vis absorption spectra were compared with those of the corresponding educts. Therefore, Nujol mulls of **1**−**3** were measured between two NaCl slides. In the case of **1**, the band at 536 nm was assigned as the π^*(Rh−Rh) → σ^*(Rh−Rh) transition, which is strongly influenced by the axial ligand.[17] A hypsochromic shift of 63 nm in comparison to that of $[Rh_2(OAc)_4]\cdot 2H_2O$ (599 nm) is observed. The electronically allowed π(Rh−O) → σ^*(Rh−O) excitation appears at 456 nm (Figure S2 in the Supporting Information, SI).[17] In the solid-state UV/vis absorption spectrum of **2**, the band localized at 442 nm should originate from the π(Ru−Ru) → π^*(Ru−Ru) transition, with a small blue shift of 23 nm in comparison to that of $[Ru_2(OAc)_4]\cdot$ 2THF (465 nm; Figure S3 in the SI).[18] In both polymers **1** and **2**, the broad bands around 330 nm should originate from the coordinated *trans*-bie ligand. In the case of polymer **3**, the lowest-energy absorption band of weak intensity is localized at 452 nm (Figure S4 in the SI) and was assigned to the δ(Mo−Mo) → δ^*(Mo−Mo) transition.[19] The more intense band around 343 nm might be caused by an overlap of the *trans*-bie absorption band and the π(Mo−Mo) → π^*(Mo−Mo) and δ(Mo−Mo) → π^*(Mo−Mo) transitions.[19]

In recent years, carbon paste electrodes (CPEs), which were first introduced in electrochemistry in 1958 by Adams,[20] have proven to be a very useful tool in the study of the electrochemical properties of coordination polymers or metal−organic frameworks.[21] Bulk-modified CPEs are the optimal choice to study their voltammetric behavior because these polymers are insoluble in water and common organic solvents. Thus, in order to investigate the electrochemical behavior of **1**−**3**, bulk-modified CPE based on the corresponding polymers (**1**-, **2**-, and **3**-CPEs) were prepared. The cyclic voltammetric behavior for **1**-, **2**-, and **3**-CPEs in H_2O, containing 0.1 M n-NH_4PF_6 as the supporting electrolyte, was then recorded (Figures S6−S8 in the SI). The cyclic voltammogram of **1**-CPE shows a quasi-reversible oxidation at $E = (E_{pc} + E_{pa})/2 = 0.92$ V vs ferrocenium/ferrocene (Fc^+/Fc). Similar values have been reported for various dinuclear paddlewheel dirhodium(II) complexes and have been assigned to the $Rh^{II}{}_2/Rh^{II}Rh^{III}$ oxidation peak.[22] In the case of **2**-CPE, an irreversible oxidation is observed at 1.01 V vs Fc^+/Fc, which presumably reflects a Ru^{II}/Ru^{III} redox couple. Concerning the cyclic voltammogram of **3**-CPE, an irreversible reduction with $E_{pc} = -1.13$ V vs Fc^+/Fc as well as an irreversible oxidation at $E_{pa} = 0.97$ V vs Fc^+/Fc are the key features to discuss. These values are comparable to values reported previously for other quadruply bonded dimolybdenum(II) compounds.[23] In summary, the electrochemical behavior of the polymers seems to be controlled by the properties of the parenting paddlewheel moieties. Especially, the rhodium-based polymer **1**, because of its quasi-reversible redox properties, appears promising regarding future molecular electronics. Thus, in analogy to $[Cu_2(O_2CCH_3)_4$(*trans*-bie)$]_n$, we also tried to deposit **1** on a highly oriented pyrolytic graphite surface. However, although it was possible to locate the rhodium polymer complex **1** on the surface, we could only detect bundles of strands (see the SI).

Preparation and Characterization of $[Cr_2(O_2CCH_3)_4$(*trans*-bie)$]_n$ (4) and $[Cr_2(O_2CCH_3)_4$(*trans*-bie)$_2]$ (5). The polymer complex **4** was synthesized by reacting chromium(II) acetate with *trans*-bie. Elemental analysis showed a stoichiometry of 1:1 $Cr_2(O_2CCH_3)_4$/*trans*-bie. The IR spectra of powder samples (KBr pellet) show that the O−C−O vibrations appear as a set of two distinctive bands in an energy region very similar to the starting material [$\tilde{\nu}_{asym}$(OCO) = 1597 cm^{-1}, $\tilde{\nu}_{sym}$(OCO) = 1437 cm^{-1}, and Δ = 160 cm^{-1} for **4**]. The solid-state UV/vis absorption spectrum of **4** shows a broad maximum around 330 nm, which is assigned to overlapping *trans*-bie and δ(Cr−Cr) → π^*(Cr−Cr) transitions of the chromium(II) acetate spectrum (Figure S5 in the SI).[24] No single crystals of the polymer could be obtained, but instead the doubly coordinated paddlewheel complex **5** was crystallized. Elemental analysis shows a stoichiometry of 1:2 $Cr_2(O_2CCH_3)_4$/*trans*-bie. The IR spectra of the compound show O−C−O vibration peaks nearly identical with those of **4**; $\tilde{\nu}_{asym}$(OCO) = 1597 cm^{-1}, $\tilde{\nu}_{sym}$(OCO) = 1436 cm^{-1}, and Δ = 159 cm^{-1} for **5**. The molecular structure of **5** is shown in Figure 4.

The paddlewheel unit consists of two chromium centers μ-bridged by four acetate ligands. Each metal atom in this unit has a distorted square-pyramidal environment, with four acetate

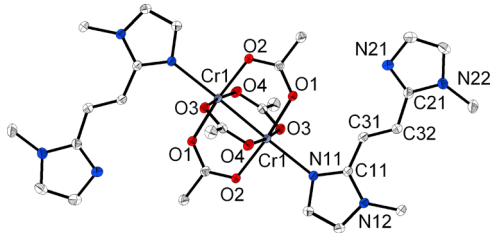

Figure 4. Molecular structure of complex **5**. Thermal ellipsoids are drawn at the 50% probability level, and hydrogen atoms have been omitted for clarity.

dx.doi.org/10.1021/ic501435a | *Inorg. Chem.* 2014, 53, 12305−12314

oxygen atoms forming the equatorial plane and one nitrogen atom of the *trans*-bie ligand. The structure of **5** has one inversion center located at the midpoint of the Cr−Cr bond. The axial M−L bond length is slightly longer in **3** than in the dinuclear complex **5**. This difference can best be explained by the different interactions of the $[Cr_2(O_2CR)_4]$ and $[Mo_2(O_2CR)_4]$ units, respectively, with the axial ligands. The tendency of $[Cr_2(O_2CR)_4]$ to bind the axial ligand is much stronger than that of $[Mo_2(O_2CR)_4]$.[4,10a] Another reason should be the oxophilic chromium center. Crystallization of polymer complexes of the general formula $[Cr_2(O_2CCH_3)_4(L)]_n$ is, to our knowledge, not reported in the literature.[4] The Cr−Cr bond length in complex **5** is longer than the M−M bonds in the pyrazine and pyridine analogous whether the Cr−N distance shows any significant differences (Table 3).[4,10b,16a]

Table 3. Structural Parameters of Various Chromium Paddlewheel Complexes $[Cr_2(O_2CCH_3)_4(L)_2]$

complex[a]	Cr−Cr [Å]	Cr−L [Å]
$[Cr_2(O_2CCH_3)_4(H_2O)_2]$[16a]	2.362(1)	2.272(3)
$[Cr_2(O_2CCH_3)_4(py)_2]$[10b]	2.369(2)	2.335(5)
$[Cr_2(O_2CCH_3)_4(pyz)_2]$[10b]	2.295(5)	2.314(10)
$[Cr_2(O_2CCH_3)_4(trans\text{-bie})_2]$ (**5**)	2.4517(5)	2.3243(12)

[a]py = pyridine; pyz = pyrazine.

Preparation and Characterization of $[Zn_3(O_2CCH_3)_6(trans\text{-bie})]_n$ (6). An attempt to crystallize the polymer compound $[Zn_2(O_2CCH_3)_4(trans\text{-bie})]_n$ by layering *trans*-bie in THF with $Zn(O_2CCH_3)\cdot H_2O$ in MeOH resulted in a coordination polymer with the molecular formula of $[Zn_3(O_2CCH_3)_6(trans\text{-bie})]_n$. The O−C−O vibrations appear in the IR spectra of powder samples (KBr pellet) as a set in the region of 1651−1422 cm^{-1}, in an energy region very similar to that of the starting acetate. The acetate protons appear as a singlet attributable to 18 protons at 1.79 ppm in ^1H NMR. The crystal structure of the polymer chain is shown in Figure 5.

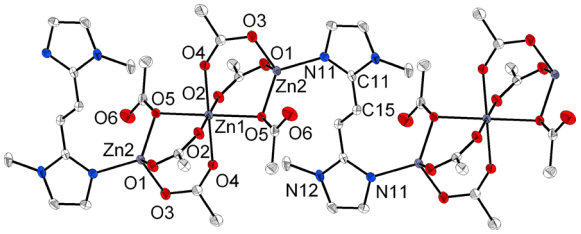

Figure 5. Cutout of the molecular structure of **6**. Thermal ellipsoids are drawn at the 50% probability level, and hydrogen atoms have been omitted for clarity.

The trinuclear zinc(II) acetate unit consists of six bridging acetate ligands and is similar to known trinuclear zinc carboxylates presented by Kim et al. with axial N- or O-donor ligands or the 1D coordination polymer published by Burzlaff et al.[25] An inversion center exists at the center of the central double bond of the *trans*-bie ligand. The central zinc is 6-fold-coordinated to six acetato groups to form a distorted octahedral geometry. The other two zinc centers are symmetrical, and each has a bridging *trans*-bie ligand and three oxygen donors from the acetato ligand to form a tetrahedrally coordinated metal center. Two different types of carboxylate coordination are found. Four acetate ligands are coordinated in a bidentate fashion by both oxygen atoms of a carboxylate group, forming syn−syn bridges between central and terminal zinc ions. The other two acetate ligands are coordinated in a monodentate fashion and function as monatomic Zn−O−Zn bridges in which one oxygen remains uncoordinated and is only involved in a weak interaction with the zinc atom [Zn2···O6 = 2.8300(15) Å].[26] The Zn···Zn distance with 3.2272(14) Å is much longer than that of similar dinuclear paddlewheel compounds.[25a,27] The Zn···Zn distance is nearly identical with those found in similar trinuclear zinc complexes.[28]

Electronic Structure and Bond Orders of Dinuclear Units within the Paddlewheel Polymers. To obtain a more comprehensive description of the nature of the M−M bonds and the electronic structure of the dinuclear units, we investigated single $[M_2(O_2CCH_3)_4(trans\text{-bie})_2]$ units with DFT and multiconfigurational state-averaged CASSCF, followed by second-order perturbation theory (CASPT2) calculations. This is based on the assumption that the electronic structures of these single $[M_2(O_2CCH_3)_4(trans\text{-bie})_2]$ units are representative for those of the polymers $[M_2(O_2CCH_3)_4(trans\text{-bie})]_n$. We first focus on the new rhodium, ruthenium, and molybdenum complexes and then also give a short description of the bonding in the copper complex reported previously.

Because in DFT the results depend strongly on the exchange and correlation functionals, we compared three different functionals (BP86,[29] B3LYP,[30] and PBE0[31]). The first is a pure density functional, while B3LYP[30] and PBE0[31] are hybrid functionals and include 20% and 25% of Hartree−Fock (HF) exchange, respectively. DFT is a single-determinantal method, and the correlation energy of the complexes is included by the correlation functional and, to a certain amount, by the HF exchange in hybrid functionals. CASSCF calculations define the multideterminantal character and therefore the static correlation, while additional CASPT2 calculations are needed to capture the dynamic correlation. The choice of the active space is crucial in CASSCF. The bonding and antibonding M−M 4d σ, δ, and two sets of π orbitals were chosen as active orbitals. Together with four carboxylate−metal σ(M−O) and σ^*(M−O) orbitals, the active space consists of n electrons in 12 orbitals (Mo, n = 12; Ru, n = 16; Rh, n = 18) and will be referred to as CASSCF(n,12) (Figure 6). Therefore, all metal-centered 4d orbitals describing the M−M bonds are included in the active space, whereas no ligand-centered orbitals were chosen. However, different previous studies showed[11a−c] that the ligands are sufficiently treated at the subsequent PT2 level.

The energy differences between the lowest spin states (singlet and triplet states) are summarized in Figure 7. The three functionals give consistent results for all three complexes with a well-defined triplet ground state for **2** (M = Ru), around 19 kcal mol^{-1} below the singlet, and even clearer singlet ground states for **1** (M = Rh), which is calculated to lie between 41 and 49 kcal mol^{-1} below the triplet state, and for **3** (M = Mo), whose singlet ground state lies 19−34 kcal mol^{-1} lower in energy than the triplet state.

CASSCF/CASPT2 agrees with the DFT results that the rhodium and molybdenum complexes have a ^1A_g ground state and the ruthenium complex has ^3A_g. The singlet−triplet gap obtained with CASPT2 is reduced to 10 kcal mol^{-1} for the ruthenium complex (Figure 7). For rhodium and molybdenum complexes, the BP86 results agree better with the CASPT2 energies than the two hybrid functionals. However, CASPT2

dx.doi.org/10.1021/ic501435a | *Inorg. Chem.* 2014, 53, 12305−12314

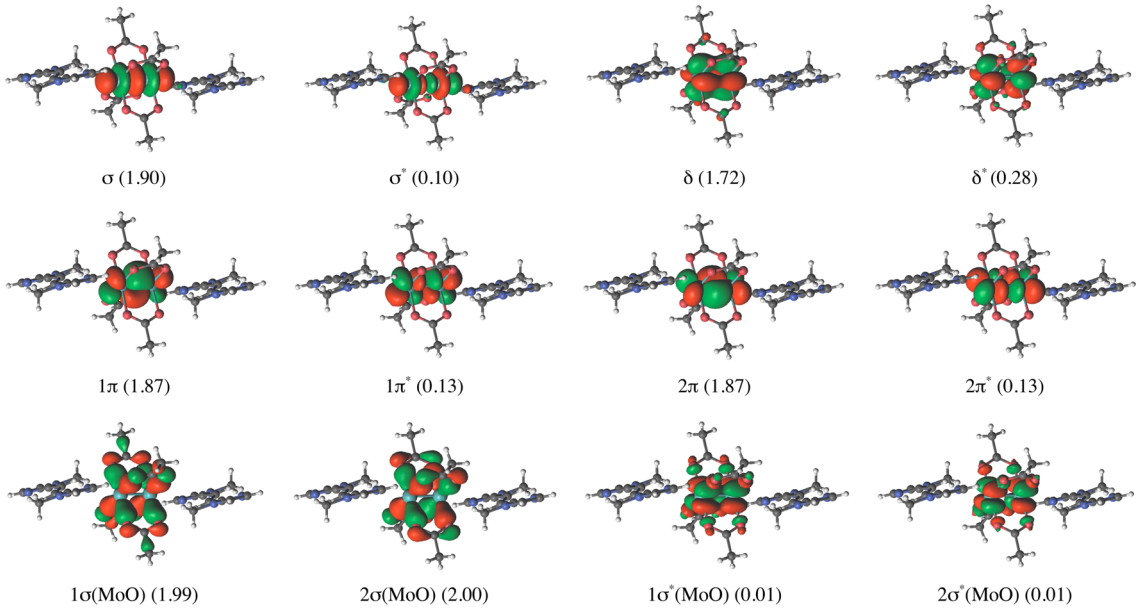

Figure 6. $[Mo_2(O_2CCH_3)_4(trans\text{-bie})_2]$ CASSCF(12,12) ^1A_g active orbitals (occupation numbers in parentheses). Active orbital sets for M = Rh and Ru can be found in the SI.

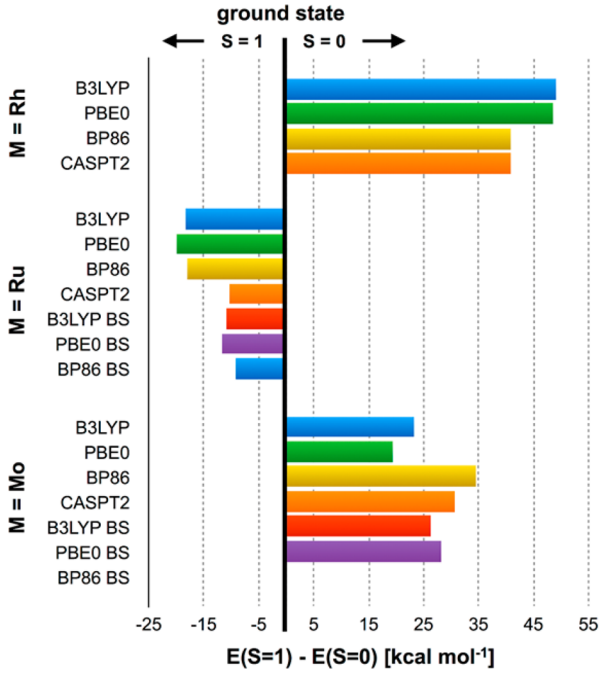

Figure 7. Energy difference between the lowest singlet and triplet states of complexes $[M_2(O_2CCH_3)_4(trans\text{-bie})_2]$. BS: Energies obtained with the BS[24] methodology. No BS wave function was obtained for M = Mo with the BP86 functional.

and DFT both predict the expected singlet ground states for dinuclear molybdenum(II) carboxylate and rhodium(II) carboxylate complexes and a triplet ground state for a dinuclear ruthenium(II) carboxylate complex.[4]

The configurations with the highest contributions to the CASSCF wave functions for the lowest singlet and triplet states are summarized in Table 4. The CASSCF(12,12) wave function of the ^1A_g ground state of the molybdenum complex is dominated to 73% by a $\sigma(M{-}O)^4\sigma^2\pi^4\delta^2$ configuration, followed by the double excitation $\sigma(M{-}O)^4\ \sigma^2\pi^4\delta^{*2}$ with 8%. The ^3A_g state corresponds to a $\delta \rightarrow \delta^*$ excitation.

The ^3A_g state of the ruthenium complex is dominated by a $\sigma(M{-}O)^4\sigma^2\pi^4\delta^2\delta^{*2}\pi^{*2}$ configuration (83%). This is consistent with structural considerations and theoretical evidence on different dinuclear ruthenium(II) carboxylate complexes, as summarized in ref 4. The first singlet state has strong multiconfigurational character, and the electrons occupy either one (51%) or the other (16%) of the two π^* orbitals. The lowest singlet and triplet states differ in configurations of the same sets of orbitals in both complexes $[Rh_2(O_2CCH_3)_4(trans\text{-bie})_2]$ and $[Ru_2(O_2CCH_3)_4(trans\text{-bie})_2]$. Furthermore, the triplet states have only one dominant configuration, with weights above 80% in both cases. This indicates that the triplet high-spin states should be described well by a single-determinant DFT wave function. However, the multiconfigurational low-spin states may be better described by the broken-symmetry (BS) solution introduced by Noodleman within the DFT framework.[32] The idea behind this approach is that the variationally determined single-determinant BS state is not a pure spin state but a mixture of "ionic" and "neutral" contributions, as pointed out by Neese.[33] The (intended) spin-contamination problem of such wave functions can be addressed by a spin-projection technique introduced by Noodleman[32a] for the weak coupling limit and improved by Yamaguchi et al.[34] for the complete coupling regime (see the Computational Details section). The singlet−triplet splittings obtained with the BS approach (Yamaguchi-corrected) for the ruthenium complex are lowered and in good agreement with the CASPT2 results (Figure 7). For complex $[Mo_2(O_2CCH_3)_4(trans\text{-bie})_2]$, the BS results with the hybrid functionals are also closer to the CASPT2 results, confirming that the closed-shell singlet is too high in energy. However, in the case of the pure BP86 functional, the BS method converged to the closed-shell wave function. Additional tests were performed to confirm the stability of this wave function (see the SI). This behavior may be attributable to the overly delocalized nature of pure DFT and the overly local nature of

dx.doi.org/10.1021/ic501435a | Inorg. Chem. 2014, 53, 12305−12314

Table 4. CASSCF Configurations of the Lowest Singlet and Triplet States of $[M_2(O_2CCH_3)_4(trans\text{-bie})_2]$

complex	weight [%]	configuration	state
$[Rh_2(O_2CCH_3)_4(trans\text{-bie})_2]$	88	$\sigma(M-O)^4\sigma^2\pi^4\delta^2\delta^{*2}\pi^{*4}$	^1A_g
	59	$\sigma(M-O)^4\sigma^2\pi^4\delta^2\delta^{*2}\pi^{*3}\sigma^*(M-O)^1$	^3A_u
	19	$\sigma(M-O)^4\sigma^2\pi^3\delta^2\delta^{*2}\pi^{*4}\sigma^*(M-O)^1$	
$[Ru_2(O_2CCH_3)_4(trans\text{-bie})_2]$	83	$\sigma(M-O)^4\sigma^2\pi^4\delta^2\delta^{*2}\pi^{*2}$	^3A_g
	51	$\sigma(M-O)^4\sigma^2\pi^4\delta^2\delta^{*2}1\pi^{*2}2\pi^{*0}$	^1A_g
	16	$\sigma(M-O)^4\sigma^2\pi^4\delta^2\delta^{*2}1\pi^{*0}2\pi^{*2}$	
	9	$\sigma(M-O)^4\sigma^2\pi^4\delta^2\delta^{*2}1\pi^{*1}2\pi^{*1}$	
$[Mo_2(O_2CCH_3)_4(trans\text{-bie})_2]$	73	$\sigma(M-O)^4\sigma^2\pi^4\delta^2$	^1A_g
	8	$\sigma(M-O)^4\sigma^2\pi^4\delta^{*2}$	
	80	$\sigma(M-O)^4\sigma^2\pi^4\delta^1\delta^{*1}$	^3A_u

Table 5. MBOs Calculated between the Metal Centers in $[M_2(O_2CCH_3)_4(trans\text{-bie})_2]$ Calculated with Different Functionals Compared to the EBO from CASSCF[a]

		CASSCF EBO				MBO		
	FSR exp	σ	π	δ	total	BP86	B3LYP	PBE0
Rh−Rh	0.963	0.82	0.00	0.01	0.83	0.76	0.77	0.80
Ru−Ru	0.916	0.87	0.81	0.00	1.68	1.70	1.73	1.76
Mo−Mo	0.814	0.90	1.74	0.72	3.36	3.32	3.30 (3.43)	3.16 (3.48)

[a]In the case of molybdenum, the MBOs obtained from the closed-shell wave function are given in parentheses. FSR is explained in the text.

Table 6. MBOs Calculated with Different Functionals for M−L Interactions in $[M_2(O_2CCH_3)_4(trans\text{-bie})_2]$[a]

	BP86			B3LYP			PBE0		
	Mo	Ru	Rh	Mo	Ru	Rh	Mo	Ru	Rh
M−N	0.20	0.29	0.33	0.18 (0.18)	0.26	0.29	0.20 (0.20)	0.28	0.32
M−O	0.60	0.51	0.52	0.52 (0.57)	0.45	0.46	0.55 (0.57)	0.48	0.49

[a]For M = Mo, the MBOs obtained from the closed-shell wave function are given in parentheses.

HF, which makes a BS solution more likely with increasing HF exchange in hybrid functionals.[35]

On the basis of the wave functions obtained, we can now proceed to analyze the different M−M bonds. The M−M bond orders obtained at different levels of theory are summarized in Table 5. The MBOs all lie below the maximum possible formal M−M bond orders. A theoretical single bond in the rhodium complex $[Rh_2(O_2CCH_3)_4(trans\text{-bie})_2]$ and a double bond in the ruthenium complex $[Ru_2(O_2CCH_3)_4(trans\text{-bie})_2]$ are consistently reduced to bond orders of 0.8 and 1.7, respectively. However, the bond order of the Mo−Mo bond in complex $[Mo_2(O_2CCH_3)_4(trans\text{-bie})_2]$ is slightly more dependent on the functional but in all cases much lower than the maximum formal bond order of four in a full quadruple bond. Interestingly, the bond orders of the BS wave functions for the hybrid functionals are the lowest obtained, while their closed-shell counterparts have higher MBOs.

The MBO agrees well with the CASSCF EBO for all three complexes, with bond orders of approximately 0.8 for M = Rh, 1.7 for M = Ru. and 3.4 for M = Mo. The closed-shell singlet states calculated with DFT give MBOs higher than the EBO values, while those calculated from the BS wave functions are in good agreement.

The EBO can also be calculated for individual bonding and antibonding orbital pairs. In the case of the molybdenum complex, σ, π, and δ orbital interactions all contribute to the total bond order with decreasing values. The additional four electrons in the case of the ruthenium complex $[Ru_2(O_2CCH_3)_4(trans\text{-bie})_2]$ lead to zero bonding between δ orbitals because the antibonding orbital is filled completely. Only σ contributions can be found for the rhodium complex $[Rh_2(O_2CCH_3)_4(trans\text{-bie})_2]$ because all π- and δ-bonding and antibonding orbitals are filled.

The bond length itself is not suitable to compare M−M bonds in a series comparing different metals because of the different atomic sizes. Therefore, the formal shortness ratio (FSR)[4] was introduced. The FSR is the M−M bond length divided by the sum of their single-bond metallic radii defined by Pauling.[36] In this work, we used the revised[37] single-bond metallic radii. $[Mo_2(O_2CCH_3)_4(trans\text{-bie})_2]$ has the smallest FSR (Table 5), which is in agreement with the highest bond order. The FSR of $[Ru_2(O_2CCH_3)_4(trans\text{-bie})_2]$ is slightly smaller than the FSR of $[Rh_2(O_2CCH_3)_4(trans\text{-bie})_2]$. Therefore, the picture obtained by our calculations is also reflected in the FSR.

The M−L bond orders are summarized in Table 6. The M−O bond orders do not vary much between the different transition metals; however, the Mo−O bonds gave the highest values, despite their bond lengths being marginally longer (about 0.06 Å) than Ru−O and Rh−O. The M−N bond orders show a clear trend. The MBO decreases in the order Rh > Ru > Mo, in agreement with the trends inferred from geometrical criteria; the bond lengths increase, and the N−M−M angles deviate more from linearity in the same order. A possible bonding between the metals in the copper(II) acetate, which is the starting material of the copper(II) polymer described earlier,[6] has been discussed in detail.[38]

Magnetic measurements on copper paddlewheel complexes indicated a very weak antiferromagnetic coupling between the metals,[38a,39] and recent theoretical investigations by Neese et al.

dx.doi.org/10.1021/ic501435a | Inorg. Chem. 2014, 53, 12305−12314

and also from Klopper et al. showed the difficulties in predicting the coupling constants or zero-field splitting.[40] We use the same minimum active space of two electrons in two σ^*(M−O) orbitals for our CASSCF/CASPT2 calculations on the copper complex as that used in these recent investigations (Figure 8).

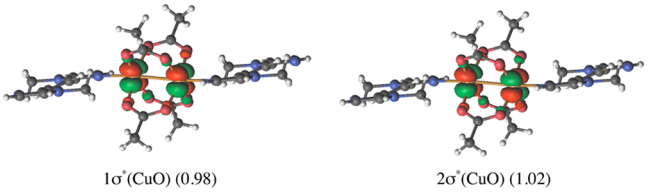

Figure 8. $[Cu_2(O_2CCH_3)_4(trans\text{-bie})_2]$ CASSCF(12,12) ^1A_g active orbitals (occupation numbers in parentheses).

Table 7. Triplet−Singlet Gap (ΔE) and Bond Orders for $[Cu_2(O_2CCH_3)_4(trans\text{-bie})_2]$[a]

	CASPT2	BP86	B3LYP	PBE0
ΔE [kcal mol^{-1}]	0.5	3.5	1.4	1.1
EBO/MBO Cu−Cu	−0.02	0.12	<0.10	<0.10
MBO Cu−N		0.51	0.49	0.51

[a]The EBO is obtained from CASSCF and the MBO from DFT.

BS DFT calculations and CASPT2(2,2) both predict a weak antiferromagnetic coupling (Table 7). The difference of 0.6−0.9 kcal mol^{-1} between CASPT2 and the hybrid functionals and a 3.0 kcal mol^{-1} difference for BP86 resemble the one reported for the hydrated and anhydrous copper(II) acetate and formate complexes.[40b] All bond orders obtained indicate zero bonding between the metal atoms. CASSCF(2,2) shows two configurations with almost equal weights (0.49 and 0.51) for the ^1A_g state. Both electrons occupy either one or the other of the two σ^*(M−O) orbitals.

The M−N coordination is the strongest in this series of *trans*-bie complexes for copper with an MBO of 0.5.

CONCLUSION

In conclusion, we have synthesized a range of metal(II) acetate paddlewheel-based coordination polymers with the *N*,*N*-donor ligand *trans*-bie and characterized several of these by X-ray structure determination. The comparison of the molecular structures of $[Cu_2(O_2CCH_3)_4(trans\text{-bie})]_n$ with those of **1**−**3** showed a correlation between the bond strength of the M−L and M−M interactions. The stronger the M−M bond in the paddlewheel unit, the weaker the bond between the metal atom and coordinating nitrogen donor. Analysis of single units of $[Mo_2(O_2CCH_3)_4(trans\text{-bie})_2]$ using CASSCF/CASPT2 and DFT calculations revealed a weakening of the possible quadruple bond, which is mainly attributable to weakly overlapping δ orbitals and a resulting EBO of 3.3. The calculated M−M bond orders in $[Rh_2(O_2CCH_3)_4(trans\text{-bie})_2]$ and $[Ru_2(O_2CCH_3)_4(trans\text{-bie})_2]$ indicate single and double bonds with values of 0.8 and 1.7, respectively. No significant bonding is present between the copper centers in $[Cu_2(O_2CCH_3)_4(trans\text{-bie})]_n$, as indicated by CASSCF/CASPT2 and DFT calculations on the single $[Cu_2(O_2CCH_3)_4(trans\text{-bie})_2]$ unit. According to cyclic voltammetric studies, the electrochemical behavior of the polymers seems to be similar to the parenting paddlewheel moieties. In this study, we investigated the difference of M−M bonding within the same framework in correlation with substitution of the metal centers. We will focus on the exchange of the substituents within the paddlewheel unit and the resulting influence on the corresponding polymers in further investigations.

EXPERIMENTAL SECTION

General Remarks. *trans*-bie,[6] ruthenium(II) acetate,[41] molybdenum(II) acetate[42] and chromium(II) acetate[43] were prepared by methods described in the literature. All coordination polymer syntheses were carried out under inert gas conditions, unless described otherwise. Solvents were purchased in absolute grade. The yields refer to analytically pure substances and were not optimized. ^{1}H NMR spectra: Bruker DPX 300 AVANCE; δ values relative to the residual solvent signal. UV/vis spectroscopy was performed with a Varian Cary 5G spectrometer and a Varian Cary 50 spectrometer. In order to get qualitative spectroscopic data of the polymers, Nujol mulls of **1**−**4** were measured between two NaCl slides. Electrochemical measurements were performed using an Autolab PGSTAT 100. A conventional three-electrode cell was used. Chemically bulk-modified CPEs based on the corresponding polymers (**1**-, **2**-, and **3**-CPEs) were used as working electrodes. A platinum wire was used as a counter electrode, and a silver wire was used as a pseudoreference electrode. IR spectra: Varian Excalibur FTS-3500 FT-IR spectrometer; KBr matrix. Elemental analysis: Euro EA 3000 Euro Vector elemental analyzer instrument. A Bruker-Nonius Kappa CCD was used for X-ray structure determination.

Synthesis. *$[Rh_2(O_2CCH_3)_4(trans\text{-bie})]_n$ (**1**).* In a test tube, under air, a solution of ligand *trans*-bie (40.0 mg, 0.209 mmol) in MeCN (10 mL) was added to a solution of $[Rh_2(O_2CCH_3)_4]\cdot 2H_2O$ (100 mg, 0.209 mmol) in MeCN (10 mL). Immediately, a pink solid that formed was separated by filtration, washed with MeCN (3 × 10 mL), and dried in a vacuum to yield a pink powder (56.0 mg, 0.089 mmol, 42%). Crystals of the compound were obtained by layering $[Rh_2(O_2CCH_3)_4]\cdot 2H_2O$ in THF with *trans*-bie in MeOH. Mp: 284 °C (dec). Elem anal. Calcd for $C_{18}H_{24}Rh_2N_4O_8$ (630.22 g mol^{-1}): C, 34.30; H, 3.84; N, 8.89. Found: C, 34.36; H, 3.67; N, 9.05. IR (KBr): $\tilde{\nu}$ 2927 (w, CH), 1592 (s, CO_2 asym), 1530 (w), 1494 (w), 1420 (m, CO_2 sym), 1357 (w), 1342 (w), 1293 (w), 1277 (w), 1262 (w), 1223 (w), 1151 (m), 1047 (w), 1026 (w), 984 (w), 939 (w), 841 (w), 765 (w) 744 (w), 720 (m), 694 (m), 673 (w), 626 (w), 591 (w), 524 (w) cm^{-1}.

*$[Ru_2(O_2CCH_3)_4(trans\text{-bie})]_n$ (**2**).* In a Schlenk tube, a solution of ligand *trans*-bie (37.0 mg, 0.200 mmol) in THF (5 mL) was added to a solution of $[Ru_2(O_2CCH_3)_4]\cdot 2THF$ (115 mg, 0.200 mmol) in THF (5 mL). After 1 h, the brown solid that formed was separated by filtration, washed with THF (5 mL) and Et_2O (5 mL), and dried in a vacuum to yield a brown powder (89.0 mg, 0.141 mmol, 71%). Crystals of the compound were obtained by layering $[Ru_2(O_2CCH_3)_4]\cdot 2THF$ in THF with *trans*-bie in MeCN. Mp: 276 °C (dec). Elem anal. Calcd for $C_{18}H_{24}Ru_2N_4O_8$ (630.22 g mol^{-1}): C, 34.51; H, 3.96; N, 8.94. Found: C, 34.35; H, 3.60; N, 8.03. IR (KBr): $\tilde{\nu}$ 3257 (w, CH), 2961 (w, CH), 1569 (s, CO_2 asym), 1533 (w), 1493 (m), 1453 (m), 1429 (s, CO_2 sym), 1343 (w), 1292 (w), 1277 (w), m 1147 (w), 1045 (w), 982 (w), 937 (w), 764 (w), 745 (w), 721 (w), 684 (w), 672 (w), 620 (w), 573 (w) cm^{-1}.

*$[Mo_2(O_2CCH_3)_4(trans\text{-bie})]_n$ (**3**).* In a Schlenk tube, a solution of ligand *trans*-bie (79.0 mg, 0.420 mmol) in THF (10 mL) was added to a solution of $[Mo_2(O_2CCH_3)_4]$ (60.0 mg, 0.140 mmol) in THF (22 mL). After 20 min, the yellow solid that formed was separated by filtration, washed with THF (2 × 10 mL), and dried in a vacuum to yield a yellow powder (16.0 mg, 0.020 mmol, 19%). Crystals of the compound were obtained by layering $[Mo_2(O_2CCH_3)_4]$ in THF with *trans*-bie in MeCN. Mp: 209 °C (dec). Elem anal. Calcd for $C_{18}H_{24}Mo_2N_4O_8$ (616.33 g mol^{-1}): C, 35.08; H, 3.92; N, 9.09. Found: C, 35.26; H, 4.04; N, 9.46. IR (KBr): $\tilde{\nu}$ 3116 (w, CH), 2928 (w, CH), 1645 (s), 1527 (w, CO_2 asym), 1473 (w), 1459 (s), 1433 (w, CO_2 sym), 1420 (w), 1350 (s), 1286 (s), 1276 (m), 1130 (m), 1043 (s),

dx.doi.org/10.1021/ic501435a | Inorg. Chem. 2014, 53, 12305−12314

Table 8. Crystal Data and Refinement Details

	1	2	3	5	6
empirical formula	$C_{27}H_{36}N_6O_{12}Rh_3{\cdot}2MeOH$	$C_9H_{12}N_2O_4Ru{\cdot}0.5THF$	$C_9H_{12}N_2O_4Mo$	$C_{28}H_{36}Cr_2N_8O_8$	$C_{11}H_{15}N_2O_6Zn_{1.5}$
fw [g mol^{-1}]	1009.43	349.33	308.15	716.65	369.3
cryst syst	monoclinic	triclinic	monoclinic	orthorhombic	triclinic
space group, Z	$P2_1/c$, 4	$P\bar{1}$	$P2_1/c$, 4	$Pbca$	$P\bar{1}$, 2
a [Å]	15.9732(17)	8.2774(8)	9.8956(1)	8.2265(6)	8.5151(17)
b [Å]	8.3335(9)	8.3739(17)	13.8296(1)	18.7004(13)	9.4623(19)
c [Å]	29.297(3)	10.5985(11)	8.6218(1)	20.32978(14)	10.267(2)
α [deg]	90	105.369(12)	90	90	68.04(3)
β [deg]	101.457(2)	107.452(7)	107.01	90	68.92(3)
γ [deg]	90	93.312(10)	90	90	70.41(3)
V [Å^3]	3822.1(7)	668.18(17)	1128.30(2)	3127.5(4)	696.3(2)
R1, wR2 (overall)	0.0374, 0.0823	0.0924, 0.2228	0.0184, 0.0446	0.0383, 0.0802	0.0207, 0.0503
GOF on F^2	1.045	1.015	1.058	1.076	1.071

1020 (s), 960 (m), 928 (s), 874 (s), 772 (m), 727 (m), 672 (m), 663 (m), 631 (s), 572 (s), 518 (s) cm^{-1}.

$[Cr_2(O_2CCH_3)_4(trans\text{-}bie)]_n$ ***(4)***. In a Schlenk tube, a solution of ligand *trans*-bie (34.0 mg, 0.186 mmol) in MeCN (20 mL) was added to a solution of $[Cr_2(O_2CCH_3)_4]{\cdot}2H_2O$ (70.0 mg, 0.186 mmol) in MeCN (50 mL). Immediately, a violet solid that formed was separated by filtration, washed with MeCN (5 mL), and dried in a vacuum to yield a violet powder (42.0 mg, 0.080 mmol, 44%). Mp: 76 °C (dec). Elem anal. Calcd for $C_{18}H_{24}Cr_2N_4O_8$ (528.40 g mol^{-1}): C, 40.91; H, 4.58; N, 10.60. Found: C, 40.84; H, 4.82; N, 10.67. IR (KBr): $\tilde{\nu}$ 2924 (m, CH), 1737 (w), 1597 (s, CO_2 asym), 1437 (s, CO_2 sym), 1344 (w), 1290 (w), 1149 (w), 1048 (w), 1031 (w), 992 (w), 935 (w), 860 (w), 781 (w), 752 (w), 728 (m), 678 (m), 622 (w), 523 (w) cm^{-1}.

$[Cr_2(O_2CCH_3)_4(trans\text{-}bie)_2]$ ***(5)***. In a Schlenk tube, a solution of $[Cr_2(O_2CCH_3)_4]{\cdot}2H_2O$ (20.0 mg, 0.038 mmol) in THF (5 mL) was layered with MeCN (4 mL). A solution of *trans*-bie (7.12 mg, 0.038 mmol) in MeCN (5 mL) was deposed on top of it. After 2 days, the red crystals were collected and dried in an oil pump vacuum to give a red powder (11.0 mg, 0.015 mmol, 40%). Crystals of the compound were obtained from the reaction solution. Mp: 63 °C (dec). Elem anal. Calcd for $C_{28}H_{36}Cr_2N_8O_8$ (716.63 g mol^{-1}): C, 46.93; H, 5.06; N, 15.64. Found (measured crystals): C, 46.96; H, 4.52; N, 14.93. IR (KBr): $\tilde{\nu}$ 3115 (w, CH), 3053 (w, CH), 2938 (w, CH), 1597 (s, CO_2 asym), 1526 (w), 1514 (w), 1481 (w), 1473 (w), 1456 (m), 1436 (s, CO_2 sym), 1416 (m), 1352 (w), 1344 (m), 1308 (w), 1289 (w), 1268 (w), 1149 (w), 1132 (w), 1085 (w), 1051 (w), 1032 (w), 992 (w), 934 (w), 859 (w), 844 (w), 781 (w), 751 (w), 728 (m), 693 (w), 678 (w), 622 (w), 523 (w) cm^{-1}.

$[Zn_3(O_2CCH_3)_6(trans\text{-}bie)]_n$ ***(6)***. In a test tube, under air, a solution of $Zn(O_2CCH_3){\cdot}H_2O$ (100 mg, 0.45 mmol) in MeOH (2 mL) was layered with a solution of *trans*-bie (85.8 mg, 0.45 mmol) in THF (15 mL). After 2 days, the white crystals were collected and dried in an oil pump vacuum to give a white powder (21.0 mg, 0.028 mmol, 6%). Crystals of the compound were obtained from the reaction solution. Mp: 255 °C (dec). Elem anal. Calcd for $C_{22}H_{30}Zn_3N_4O_{12}$ (738.63 g mol^{-1}): C, 35.77; H, 4.09; N, 7.59. Found (measured crystals): C, 36.13; H, 4.09; N, 7.25. ^{1}H NMR ($CDCl_3$): δ 1.79 (s, 18 H, O_2CCH_3), 3.75 (s, 6H, CH_3), 7.05 (s, 2H, CH_{Im}), 7.29 (s, 2H, CH_{Im}), 7.36 (s, 2H, CH_2). IR (KBr): $\tilde{\nu}$ 3135 (w, CH), 3115 (w, CH), 2927 (w, CH), 1651 (m), 1592 (s), 1493 (m), 1422 (m), 1342 (w), 1299 (m), 1158 (w), 1049 (w), 1023 (w), 966 (w), 957 (w), 925 (w), 793 (w), 768 (w), 730 (w), 672 (w), 617 (w), 525 (w) cm^{-1}.

Cyclic Voltammetry and Reparation of 1-, 2-, and 3-CPEs. Cyclic voltammetry experiments were performed using an Autolab PGSTAT 100. A conventional three-electrode cell was used, using the corresponding CPEs (**1**-, **2**-, and **3**-CPEs) as working electrodes. A platinum wire was used as a counter electrode, and a silver wire was used as a pseudoreference electrode. In order to build the CPEs, bulk-modified CPEs were prepared by mixing the coordination polymers **1**−**3** (12.5% w/w) with graphite powder (57.5% w/w) by an agate mortar and pestle followed by the addition of a Nujol mull (30% w/w). The mixtures were levigated, and the homogenized mixtures were filled in micropipette tips (1 mL volume capacity, Eppendorf)[44] as electrode bodies. Electrical contact was established with a copper rod through the back of the electrode.[44] Cyclic voltammetry was performed in H_2O containing 0.1 M *n*-NH_4PF_6 as the supporting electrolyte. All solutions were deoxygenated with dinitrogen before each experiment, and a blanket of dinitrogen was used to cover the solution during the experiment. The potential values (E) were calculated using the following equation: $E = (E_{pc} + E_{pa})/2$, where E_{pc} and E_{pa} correspond to the cathodic and anodic peak potentials, respectively. The potentials are referenced to the Fc^+/Fc couple. For this purpose, ferrocene in a CPE was used as an internal standard. The ferrocene-based electrodes were prepared similarly to the polymer-based working electrodes. Five measurements were executed with ferrocene−CPEs, evaluating a standard deviation of the mean offset of 0.019 V.

Computational Details. The geometries of single $[M_2(O_2CCH_3)_4(trans\text{-}bie)_2]$ units obtained from the crystal structures were used in all calculations. DFT calculations were performed with the *ORCA 3.0*[45] program package. The def2-TZVP[46] basis set [including effective core potentials (ECPs)[46b,47] on rhodium, ruthenium, and molybdenum] in combination with the def2-TZVP/J[48] Coulomb fitting basis for the resolution of identity (for BP86[29]) was used in all calculations. The generalized gradient approximation functional BP86[29] and two hybrid functionals, PBE0[31] and B3LYP[30] (with parameters VWN-III[49] for the local part of the correlation energy), were used. A very tight self-consistent-field convergence criterion (energy change of 10^{-9} Eh) and a larger integration grid for the numerical integration (grid5) were chosen. Details of the applied BS formalism can be found in the SI. CASSCF/CASPT2 calculations were performed with the *MOLCAS 7.8* package.[50] The natural-orbital-type basis sets ANO-RCC-VTZP[51] for the metal atoms and ANO-RCC-VDZP[52] for all other atoms were used. The Douglas−Kroll−Hess[53] Hamiltonian was used to include scalar relativistic effects. To speed up the calculation of the two-electron integrals, the Cholesky decomposition method[54] with an atomic compact basis set was applied. An imaginary shift of 0.1 units was added to the external part of the zero-order Hamiltonian to prevent intruder states in the CASPT2 calculations. The C_i symmetry of the complexes was used in the calculations. The EBOs were calculated from the sums of the occupation numbers of bonding (η_b) and antibonding (η_a) orbitals (eq 1).

$$\mathrm{EBO} = \frac{\eta_b - \eta_a}{2} \tag{1}$$

X-ray Crystal Structure Analyses. A Bruker-Nonius Kappa CCD diffractometer was used for data collection (graphite monochromator, Mo Kα radiation, λ = 0.710 73 Å). Single crystals of **1**, **3**, **5**, and **6** were coated with perfluoropolyether, picked with a glass fiber, and immediately mounted in the nitrogen cold gas stream of the diffractometer. The single crystal of **2** was mounted with glue. The

dx.doi.org/10.1021/ic501435a | *Inorg. Chem.* 2014, 53, 12305−12314

structures were solved by using direct methods and refined with full-matrix least squares against F^2 (*SHELX-97*).[55] A weighting scheme was applied in the last steps of the refinement with $w = 1/[\sigma^2(F_o^2) + (aP)^2 + bP]$ and $P = [2F_c^2 + \max(F_0^2,0)]/3$. Hydrogen atoms were included in their calculated positions and refined in a riding model. The asymmetric unit of **1** contains two molecules of MeOH, of which one is disordered over two positions. The asymmetric unit of **2** contains half a THF molecule, which is disordered over two positions. Crystal data and refinement details are shown in Table 8. The structure pictures were prepared with the program *Diamond 2.1e*.[56] CCDC 997497−997501 contain the supplementary crystallographic data for this paper (see the SI). These data can also be obtained free of charge from the Cambridge Crystallographic Data Centre via www.ccdc.cam.ac.uk/data_request/cif.

■ ASSOCIATED CONTENT

Supporting Information

CIF files giving crystallographic data for **1**−**3**, **5**, and **6**, selected bond lengths, extended crystal data and refinement details, STM measurements, qualitative UV/vis spectra of **1**−**4**, cyclic voltammograms of **1**-CPE, **2**-CPE, and **3**-CPE, detailed tables of DFT Cartesian coordinates, CASSCF/CASPT2 active orbitals, and a summary of the lowest excited states and BS DFT calculations. This material is available free of charge via the Internet at http://pubs.acs.org.

■ AUTHOR INFORMATION

Corresponding Authors

*E-mail: Tim.Clark@fau.de.
*E-mail: Nicolai.Burzlaff@fau.de.

Present Addresses

[⊥]P.O.D.: Max-Planck-Institut für Kohlenforschung, Kaiser-Wilhelm-Platz 1, 45470 Mülheim an der Ruhr, Germany.
[∥]J.T.: Institute of Inorganic Chemistry 1, Ulm University, Albert-Einstein-Allee 11, 89081 Ulm, Germany.

Author Contributions

[‡]These authors contributed equally.

Notes

The authors declare no competing financial interest.

■ ACKNOWLEDGMENTS

This work was supported by the Cluster of Excellence "Engineering of Advanced Materials" financed by Deutsche Forschungsgemeinschaft and by the Bavarian Free State as part of the "Solar Technologies go Hybrid" (SolTech) initiative.

■ REFERENCES

(1) (a) Blake, A. J.; Champness, N. R.; Hubberstey, P.; Li, W.-S.; Withersby, M. A.; Schröder, M. *Coord. Chem. Rev.* **1999**, *183*, 117−138. (b) Barnett, S. A.; Champness, N. R. *Coord. Chem. Rev.* **2003**, *246*, 145−168.

(2) (a) Leong, W. L.; Vittal, J. J. *Chem. Rev.* **2010**, *111*, 688−764. (b) Robin, A. Y.; Fromm, K. M. *Coord. Chem. Rev.* **2006**, *250*, 2127−2157.

(3) (a) Ruben, M.; Lehn, J.-M.; Muller, P. *Chem. Soc. Rev.* **2006**, *35*, 1056−1067. (b) Mas-Ballesté, R.; Castillo, O.; Sanz Miguel, P. J.; Olea, D.; Gómez-Herrero, J.; Zamora, F. *Eur. J. Inorg. Chem.* **2009**, *2009*, 2875−2875. (c) Petukhov, K.; Alam, M. S.; Rupp, H.; Strömsdörfer, S.; Müller, P.; Scheurer, A.; Saalfrank, R. W.; Kortus, J.; Postnikov, A.; Ruben, M.; Thompson, L. K.; Lehn, J. M. *Coord. Chem. Rev.* **2009**, *253*, 2387−2398. (d) Olea, D.; Alexandre, S. S.; Amo-Ochoa, P.; Guijarro, A.; de Jesús, F.; Soler, J. M.; de Pablo, P. J.; Zamora, F.; Gómez-Herrero, J. *Adv. Mater.* **2005**, *17*, 1761−1765. (e) Cook, T. R.; Zheng, Y.-R.; Stang, P. J. *Chem. Rev.* **2012**, *113*, 734−777.

(4) Cotton, F. A.; Murillo, C. A.; Walton, R. A. *Multiple Bonds between Metal Atoms*; Springer: Boston, MA, 2005.

(5) Bennett, M. J.; Caulton, K. G.; Cotton, F. A. *Inorg. Chem.* **1969**, *8*, 1−6.

(6) Fischer, N. V.; Alam, M. S.; Jum'h, I.; Stocker, M.; Fritsch, N.; Dremov, V.; Heinemann, F. W.; Burzlaff, N.; Müller, P. *Chem.—Eur. J.* **2011**, *17*, 9293−9297.

(7) Das, A.; Todorov, I.; Dey, S. K.; Mitra, S. *Inorg. Chim. Acta* **2006**, *359*, 2041−2046.

(8) Shustorovich, E. M.; Porai-Koshits, M. A.; Buslaev, Y. A. *Coord. Chem. Rev.* **1975**, *17*, 1.

(9) Miyasaka, H.; Clerac, R.; Campos-Fernandez, C. S.; Dunbar, K. R. *J. Chem. Soc., Dalton Trans.* **2001**, *0*, 858−861.

(10) (a) Handa, M.; Mikuriya, M.; Kotera, T.; Yamada, K.; Nakao, T.; Matsumoto, H.; Kasuga, K. *Bull. Chem. Soc. Jpn.* **1995**, *68*, 2567−2572. (b) Cotton, F. A.; Felthouse, T. R. *Inorg. Chem.* **1980**, *19*, 328−331.

(11) (a) Li Manni, G.; Dzubak, A. L.; Mulla, A.; Brogden, D. W.; Berry, J. F.; Gagliardi, L. *Chem.—Eur. J.* **2012**, *18*, 1737−1749. (b) Brynda, M.; Gagliardi, L.; Roos, B. O. *Chem. Phys. Lett.* **2009**, *471*, 1−10. (c) La Macchia, G.; Li Manni, G.; Todorova, T. K.; Brynda, M.; Aquilante, F.; Roos, B. O.; Gagliardi, L. *Inorg. Chem.* **2010**, *49*, 5216−22. (d) Noor, A.; Bauer, T.; Todorova, T. K.; Weber, B.; Gagliardi, L.; Kempe, R. *Chem.—Eur. J.* **2013**, *19*, 9825−32. (e) Wagner, F. R.; Noor, A.; Kempe, R. *Nat. Chem.* **2009**, *1*, 529−36. (f) Weinhold, F.; Landis, C. R. *Science* **2007**, *316*, 61−63. (g) Gagliardi, L.; Roos, B. O. *Inorg. Chem.* **2003**, *42*, 1599−1603. (h) Ferrante, F.; Gagliardi, L.; Bursten, B. E.; Sattelberger, A. P. *Inorg. Chem.* **2005**, *44*, 8476−8480. (i) Poineau, F.; Gagliardi, L.; Forster, P. M.; Sattelberger, A. P.; Czerwinski, K. R. *Dalton Trans.* **2009**, 5954−5959. (j) Poineau, F.; Forster, P. M.; Todorova, T. K.; Gagliardi, L.; Sattelberger, A. P.; Czerwinski, K. R. *Inorg. Chem.* **2010**, *49*, 6646−6654.

(12) Roos, B. O.; Borin, A. C.; Gagliardi, L. *Angew. Chem.* **2007**, *119*, 1491−1494; *Angew. Chem., Int. Ed.* **2007**, *46*, 1469−1472.

(13) (a) Mayer, I. *Chem. Phys. Lett.* **1983**, *97*, 270−274. (b) Mayer, I. *Int. J. Quantum Chem.* **1984**, *26*, 151−4.

(14) Bridgeman, A. J.; Cavigliasso, G.; Ireland, L. R.; Rothery, J. *J. Chem. Soc., Dalton Trans.* **2001**, 2095−2108.

(15) Nakamoto, K. Applications in Inorganic Chemistry. In *Infrared and Raman Spectra of Inorganic and Coordination Compounds*; John Wiley & Sons, Inc.: New York, 2008; pp 149−354.

(16) (a) Cotton, F. A.; DeBoer, B. G.; LaPrade, M. D.; Pipal, J. R.; Ucko, D. A. *Acta Crystallogr., Sect. B* **1971**, *27*, 1664−1671. (b) Brown, G. M.; Chidambaram, R. *Acta Crystallogr., Sect. B* **1973**, *29*, 2393−2403. (c) Lindsay, A. J.; Tooze, R. P.; Motevalli, M.; Hursthouse, M. B.; Wilkinson, G. *J. Chem. Soc., Chem. Commun.* **1984**, *0*, 1383b−1384. (d) Robbins, G. A.; Martin, D. S. *Inorg. Chem.* **1984**, *23*, 2086−2093.

(17) Frelek, J.; Jaźwiński, J.; Masnyk, M.; Ruśkowska, P.; Szmigielski, R. *Tetrahedron: Asymm.* **2005**, *16*, 2437−2448.

(18) Chisholm, M. H.; Christou, G.; Folting, K.; Huffman, J. C.; James, C. A.; Samuels, J. A.; Wesemann, J. L.; Woodruff, W. H. *Inorg. Chem.* **1996**, *35*, 3643−3658.

(19) Jawiczuk, M.; Górecki, M.; Suszczyńska, A.; Karchier, M.; Jaźwiński, J.; Frelek, J. *Inorg. Chem.* **2013**, *52*, 8250−8263.

(20) (a) Adams, R. N. *Anal. Chem.* **1958**, *30*, 1576. For a review, see: (b) Švancara, I.; Vytřas, K.; Kalcher, K.; Walcarius, A.; Wang, J. *Electroanalysis* **2009**, *21*, 7−28.

(21) (a) Wang, X.; Bi, Y.; Chen, B.; Lin, H.; Liu, G. *Inorg. Chem.* **2008**, *47*, 2442−2448. (b) Wang, X.; Hu, H.; Tian, A. *Cryst. Growth Des.* **2010**, *10*, 4786−4794. (c) Fu, H.; Wang, Z.; Liang, C.; Zhang, Z.; Wang, E. *Dalton Trans.* **2012**, *41*, 4084−4090. (d) Wang, X.; Luan, J.; Lin, H.; Lu, Q.; Xu, C.; Liu, G. *Dalton Trans.* **2013**, *42*, 8375−8386. (e) Wang, X.; Han, N.; Lin, H.; Tian, A.; Liu, G.; Zhang, J. *Dalton Trans.* **2014**, *43*, 2052−2060. (f) Zhao, J.-W.; Li, Y.-Z.; Ji, F.; Yuan, J.; Chen, L.-J.; Yang, G.-Y. *Dalton Trans.* **2014**, *43*, 5694−5706. (g) Wang, X.; Sui, F.; Lin, H.; Zhang, J.; Liu, G. *Cryst. Growth Des.* **2014**, *14*, 3438−3452.

(22) Amo-Ochoa, P.; Jiménez-Aparicio, R.; Perles, J.; Torres, M. R.; Gennari, M.; Zamora, F. *Cryst. Growth Des.* **2013**, *13*, 4977−4985.

(23) Majumdar, M.; Patra, S. K.; Kannan, M.; Dunbar, K. R.; Bera, J. K. *Inorg. Chem.* **2008**, *47*, 2212−2222.
(24) Rice, S. F.; Wilson, R. B.; Solomon, E. I. *Inorg. Chem.* **1980**, *19*, 3425−3431.
(25) (a) Kwak, H.; Lee, S. H.; Kim, S. H.; Lee, Y. M.; Park, B. K.; Lee, E. Y.; Lee, Y. J.; Kim, C.; Kim, S.-J.; Kim, Y. *Polyhedron* **2008**, *27*, 3484−3492. (b) Karmakar, A.; Sarma, R. J.; Baruah, J. B. *Inorg. Chem. Commun.* **2006**, *9*, 1169−1172. (c) Clegg, W.; Little, I. R.; Straughan, B. P. *Inorg. Chem.* **1988**, *27*, 1916−1923. (d) Williams, C. A.; Blake, A. J.; Hubberstey, P.; Schroder, M. *Chem. Commun.* **2005**, *0*, 5435−5437. (e) Waidmann, T.; Fritsch, N.; Tucher, J.; Rudolf, M.; Glaser, F.; Guldi, D. M.; Burzlaff, N. *CrystEngComm* **2013**, *15*, 10157−10160.
(26) Zeleňák, V.; Sabo, M.; Massa, W.; Llewellyn, P. *Inorg. Chim. Acta* **2004**, *357*, 2049−2059.
(27) Kwak, H.; Lee, S. H.; Kim, S. H.; Lee, Y. M.; Park, B. K.; Lee, Y. J.; Jun, J. Y.; Kim, C.; Kim, S.-J.; Kim, Y. *Polyhedron* **2009**, *28*, 553−561.
(28) Clegg, W.; Little, I. R.; Straughan, B. P. *J. Chem. Soc., Dalton Trans.* **1986**, *0*, 1283−1288.
(29) (a) Andzelm, J.; Wimmer, E. *J. Chem. Phys.* **1992**, *96*, 1280−1303. (b) Perdew, J. P. *Phys. Rev. B* **1986**, *33*, 8822−8824.
(30) (a) Becke, A. D. *J. Chem. Phys.* **1993**, *98*, 5648−5652. (b) Lee, C.; Yang, W.; Parr, R. G. *Phys. Rev. B* **1988**, *37*, 785−789. (c) Miehlich, B.; Savin, A.; Stoll, H.; Preuss, H. *Chem. Phys. Lett.* **1989**, *157*, 200−206.
(31) (a) Perdew, J. P.; Burke, K.; Ernzerhof, M. *Phys. Rev. Lett.* **1997**, *78*, 1396−1396. (b) Adamo, C.; Barone, V. *J. Chem. Phys.* **1999**, *110*, 6158−6170.
(32) (a) Noodleman, L. *J. Chem. Phys.* **1981**, *74*, 5737. (b) Noodleman, L.; Davidson, E. R. *Chem. Phys.* **1986**, *109*, 131−143.
(33) Neese, F. *J. Phys. Chem. Solids* **2004**, *65*, 781−785.
(34) (a) Yamaguchi, K.; Fukui, H.; Fueno, T. *Chem. Lett.* **1986**, *15*, 625−628. (b) Soda, T.; Kitagawa, Y.; Onishi, T.; Takano, Y.; Shigeta, Y.; Nagao, H.; Yoshioka, Y.; Yamaguchi, K. *Chem. Phys. Lett.* **2000**, *319*, 223−230.
(35) Neese, F. *Coord. Chem. Rev.* **2009**, *253*, 526−563.
(36) Pauling, L. *J. Am. Chem. Soc.* **1947**, *69*, 542−553.
(37) Pauling, L. *The Nature of the Chemical Bond*, 3rd ed.; Cornell University Press: Ithaca, NY, 1960; p 403.
(38) (a) Figgis, B. N.; Martin, R. L. *J. Chem. Soc.* **1956**, 3837−3846. (b) Ross, I. G. *Trans. Faraday Soc.* **1959**, *55*, 1057−1063. (c) Ross, I. G.; Yates, J. *Trans. Faraday Soc.* **1959**, *55*, 1064−1069.
(39) (a) Guedel, H. U.; Stebler, A.; Furrer, A. *Inorg. Chem.* **1979**, *18*, 1021−1023. (b) Elmali, A. *Turk. J. Phys.* **2000**, *24*, 667−672.
(40) (a) Maurice, R. m.; Sivalingam, K.; Ganyushin, D.; Guihéry, N.; de Graaf, C.; Neese, F. *Inorg. Chem.* **2011**, *50*, 6229−6236. (b) Vogiatzis, K. D.; Klopper, W.; Mavrandonakis, A.; Fink, K. *ChemPhysChem* **2011**, *12*, 3307−3319.
(41) Kuznetsov, V. F.; Yap, G. P. A.; Alper, H. *Organometallics* **2001**, *20*, 1300−1309.
(42) Holste, G.; Schäfer, H. *Z. Anorg. Allg. Chem.* **1972**, *391*, 263−270.
(43) Brauer, G. *Lehrbuch der Präparativen Anorganischen Chemie*; Enke Verlang: Stuttgart, Germany, 1981.
(44) Vytřas, K.; Metalka, R. *J. Serb. Chem. Soc.* **2009**, *74*, 1021−1033.
(45) Neese, F. *Wiley Interdiscip. Rev.: Comput. Mol. Sci.* **2012**, *2*, 73−78.
(46) (a) Schäfer, A.; Horn, H.; Ahlrichs, R. *J. Chem. Phys.* **1992**, *97*, 2571−2577. (b) Weigend, F.; Ahlrichs, R. *Phys. Chem. Chem. Phys.* **2005**, *7*, 3297−3305.
(47) Andrae, D.; Häußermann, U.; Dolg, M.; Stoll, H.; Preuß, H. *Theor. Chim. Acta* **1990**, *77*, 123−141.
(48) Weigend, F. *Phys. Chem. Chem. Phys.* **2006**, *8*, 1057−1065.
(49) Vosko, S. H.; Wilk, L.; Nusair, M. *Can. J. Phys.* **1980**, *58*, 1200−1211.
(50) Aquilante, F.; De Vico, L.; Ferré, N.; Ghigo, G.; Malmqvist, P.-å.; Neogrády, P.; Pedersen, T. B.; Pitoňák, M.; Reiher, M.; Roos, B. O.; Serrano-Andrés, L.; Urban, M.; Veryazov, V.; Lindh, R. *J. Comput. Chem.* **2010**, *31*, 224−247.
(51) Roos, B. O.; Lindh, R.; Malmqvist, P.-Å.; Veryazov, V.; Widmark, P.-O. *J. Phys. Chem. A* **2005**, *109*, 6575−6579.
(52) Roos, B. O.; Lindh, R.; Malmqvist, P.-Å.; Veryazov, V.; Widmark, P.-O. *J. Phys. Chem. A* **2003**, *108*, 2851−2858.
(53) Hess, B. A. *Phys. Rev. A* **1986**, *33*, 3742−3748.
(54) (a) Aquilante, F.; Pedersen, T. B.; Lindh, R. *J. Chem. Phys.* **2007**, *126*, 194106. (b) Aquilante, F.; Malmqvist, P.-Å.; Pedersen, T. B.; Ghosh, A.; Roos, B. O. *J. Chem. Theory Comput.* **2008**, *4*, 694−702. (c) Aquilante, F.; Pedersen, T. B.; Lindh, R.; Roos, B. O.; Sánchez de Merás, A.; Koch, H. *J. Chem. Phys.* **2008**, *129*, 024113.
(55) Sheldrick, G. *Acta Crystallogr., Sect. A* **2008**, *64*, 112−122.
(56) Pennington, W. T. *J. Appl. Crystallogr.* **1999**, *32*, 1028−1029.